

# Development of an IMS Type Device for Volatile Organic Compounds Detection: Simulation and Comparison of the Ion Distributions

Guillermo P. Ortiz<sup>\*,a</sup>, Carlos A. Rinaldi<sup>b,1</sup>, Norberto G. Boggio<sup>b,1</sup>, Juan Vorobioff<sup>b</sup>, Juan J. Ortiz<sup>b</sup>, S. Gómez<sup>a,1</sup>, G.A. Aucar<sup>a,1</sup>, A. Lamagna<sup>b</sup>, A. Boselli<sup>b</sup>

<sup>a</sup>*Departamento de Física, Facultad de Ciencias Exactas, Universidad Nacional del Nordeste, Av. Libertad 5400 Campus-UNNE, W3404AAS Corrientes, Argentina.*

<sup>b</sup>*Instituto de Nanociencia y Nanotecnología, Comisión Nacional de Energía Atómica, CAC Av. Gral Paz 1499 San Martín, Buenos Aires, Argentina.*

---

## Abstract

Ion Mobility Spectrometry (IMS) is a well-known, sensitive and rapid technique to detect dangerous organic compounds. We propose a system in which a crown type discharge generates an ionic flux that is swept towards an array of collectors by a transverse electric field. The ions are separated as they enter the cell according to their mobility. Thus, the distribution of the charge collected at the detector assembly constitutes a *fingerprint* for each organic compound. Simulations of our cell and experiments were performed for small amounts of Acetone, Ethanol and Toluene. The dependence on the cell parameters of the current and charge versus time of flight was analyzed. Our simulation reproduces only qualitatively the experimental results. However, a PCA statistical analysis of the simulated results shows that such a fingerprint can be used to identify those compounds with certainty.

---

## 1. Introduction

The technique for identification of volatile organic compounds by differences of ion mobility is one of the most efficient techniques applied for detection of explosives, drugs and industrial toxic compounds [1]. The detection limit of this technique is found to be of the order of  $10^{-9}$  (ppb). It has a very rapid response time, which makes it very attractive for situations of high control demands. The ions of the molecule to be identified acquire a velocity under the influence of an external electric field  $\vec{E}$ . At the lowest order

---

\*Corresponding author

*Email address:* gortiz@exa.unne.edu.ar (Guillermo P. Ortiz)

<sup>1</sup>Fellow of CONICET

$$\vec{v}_E = K\vec{E}, \quad (1)$$

where  $K$  is the mobility. If the field is intense enough it has been reported [2] that one should go two orders higher (cubic) in the field dependence. A way to understand this result is by considering a power series expansion on  $\vec{E}$ . Assuming isotropy of  $K$  and applying symmetries on spatial transformations, the vectorial properties of  $\vec{v}_E$  and  $\vec{E}$  determines that only odd terms in such expansion are possibles.

Besides the interaction of the ions with the field  $\vec{E}$ , they collides with molecules of the carrier gas that flow through the detection system under a laminar flux. The explicit dependence of  $K$  on the pressure due to the carrier gas, the temperature, the ion charge, its mass and the cross section can be obtained from general considerations when the field  $\vec{E}$  is not very intense [2]. Working on the center of mass framework to describe the collisions between two bodies, and the reduced mass  $m_r = Mm/(M + m)$  where  $m$  is the mass of ions and  $M$  the mass of the molecules of the gas, the variation of the linear momentum of ion-gas system is due to the external impulse of force, *i.e.*  $qE\tau$ , being  $q$  the ion charge and  $\tau$  the characteristic time between collisions. It can thus be established that

$$v_E = qE\tau/m_r. \quad (2)$$

Furthermore  $\tau$  can be related to a collision cross section of the ion-gas system  $\Omega$  and the density of this system, which is approximately equal to the gas density  $\eta$ . Considering the characteristic length  $l = \tilde{v}\tau$  and the average rate  $\tilde{v}$  of the reduced system ion-gas between collisions, it is estimated that in the volume  $l\Omega$  a collision should typically occur. Hence  $\eta \approx 1/(l\Omega)$  and Eq. (2) can be written

$$v_E = \frac{qE}{m_r} \frac{1}{\eta\Omega\tilde{v}}. \quad (3)$$

One can approximate  $\tilde{v} \approx (3k_B T/m_r)^{1/2}$  because the kinetic energy of the ion-gas system is mainly due to thermal agitation of value  $k_B T/2$  for each degree of freedom. Then

$$v_E = \frac{qE}{\eta\Omega} \left( \frac{m+M}{mM3k_B T} \right)^{1/2}, \quad (4)$$

being  $k_B$  the Boltzman constant and  $T$  the absolute temperature. In Eq. (4) there is a factor  $3^{-1/2}$  that should be replaced by  $3(2\pi)^{1/2}/16$  when more advanced molecular calculations are considered [3].

We include such derivation here because it contains the right dependence with the physical parameters of interest and its derivation is straightforward. In the calculations presented in this work we employ instead the mobility usually reported in the literature [4, 5], which is obtained from

$$v_E/E = \frac{3q}{16\eta\Omega} \left( \frac{2\pi(m+M)}{mMk_B T} \right)^{1/2}. \quad (5)$$

This mobility is standardized at normal  $P_0$  pressures and  $T_0$  temperatures through

$$K_0 = K(T_0/T, P/P_0), \quad (6)$$

$T_0 = 273 \text{ }^\circ\text{K}$  and  $P_0$  depends on the system of unities used to refer to 1013 HPa.  $K_0$  is known as the reduced mobility.

A decade ago the identification of species by separation techniques [6] was based on the differences in the reduced mobilities given by Eq.(6). Since then substantial modifications have been made in the design and size of sensor devices. Using asymmetric electric fields in the range of radio-frequency and by micro-machining the detection cell, a field asymmetric or FA-IMS variant was proposed [7]. Identifications of up to 0.1 ppm of Toluene and also a resolution threshold of 60 ppb for a mix of gases of Acetone-Benzene and Acetone-Toluene were reported. It has been recently proposed [8] a combination of mass spectroscopy and ion mobility to improve the transmittance in an Ion Mass Mobility Spectroscopy through a focus cell by means of periodical electrostatic fields distributed on a very long arrangement of electrode rings (1m of length). It has also been proposed recently an IMS type cell by swept-field scanning [9] in which a plane and parallel detectors system produces an electric field perpendicular to the flux of the ions being detected. The operating principle of this device for mobility identification is based on the differences of the average path described by the ions within the detection cell.

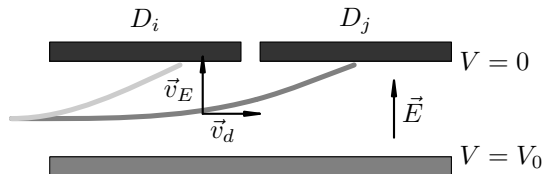


Figure 1: Average paths within the detection cell.  $D_i$ ,  $D_j$  represent two of the seven detectors contained in the cell. The detectors are earthed and the anode is kept at  $V_0$  potential. The left path corresponds to an ion with higher mobility with respect to the right path.

In Fig. 1 an example of two ion paths corresponding to ions with different mobility is given. Due to the velocity of the carrier flux, the ions reach a detection zone with velocity  $\vec{v}_d$  parallel to the detectors plane. By the action of the transversal field  $\vec{E}$ , the ions acquire, according to Eq. (1), a vertical component velocity  $\vec{v}_E$  proportional to the mobility  $K$ . By adjusting the geometrical parameters of the cell, the flux of the carrier gas and the potentials among electrodes, it is possible to obtain a typical ion distribution for each compound on the  $D_i$  and  $D_j$  detectors, where  $i \neq j = 1 \dots n$  are labels. This is characterized by a greater accumulation of charges on the detectors, whose positions measured from the gas input in the cell are more distant for ions with less mobility, as is suggested schematically in Fig. 1.

A modification in the swept-field scanning detection was recently proposed. It includes an ion-focusing just before the introduction of ions in the detection cell [10]. In this variant, the flux of both the carrier gas and the ionized gas are

separated through geometrical constrictions. This increase the precision of the positions reached by the ions in the detection cell. In that sense, the aim of such a proposal is not meant to obtain a fingerprint for each compound. Indeed it proposes that the identification shall be determined by the average time taken by each species to reach a specific detector [10]. Although the ion time of flight has been analyzed for different values of carrier gas flux and potentials between electrodes in order to evaluate the focalization conditions, it has been found in this work that identification of species by statistical analysis of their traces on detectors is more accurate if few restrictions are imposed by operational conditions, *i.e.*, work pressure and non-radioactive ionization method. Furthermore, due to the fact of a very high difference of electric potential generated by the crown effect, fragments of the molecule to identify are produced, each one with a different mobility. In our work we have found that this effect is consistent with the formation of a fingerprint for each species at the moment of measuring the total charge deposited on the detector assembly.

Basically, the main idea behind a fingerprint identification is the following: A system is designed in such a way that traces of given chemical components are well defined under specific operating conditions. With this purpose, numerical simulations are first performed, which allow us to identify these specific conditions. The algorithm used to simulate the ion detection system has proven to be sufficiently robust for the design of ion mobility detection cells [11]. Furthermore in our work, the design of an experimental prototype is analyzed for obtaining traces of Ethanol, Acetone and Toluene. The statistical study of these traces was performed by the principal components analysis [12], known as PCA (acronyms from Principal Components Analysis), which was used earlier on similar identifications within the design of an electronic sniffer [13].

We present our work in the following way. In Section 2 we describe the experimental configuration of the prototype device and the procedure we followed for the measurement of signals in the identification of three different chemical species. In Section 3 we present a brief description of the algorithm used for the simulation of ion paths. We divided Section 4 in four parts in order to show the experimental results in Subsection 4.1, time of flight simulations in Subsection 4.2 and collected charges in Subsection 4.3. In Subsection 4.4 we present the analysis of principal components and Section 5 is devoted to the main conclusions.

## 2. Experimental device

An experimental device has been designed as indicated in Fig. 2. It consists of three principal parts: i) the carrier gas flux inlet, ii) the ionization chamber and iii) the detection cell. The sample is introduced as a gas in the ionization chamber together with the carrier gas where, through a type of crown discharge, is ionized. The pointer shaped electrode, shown in the central part of Fig. 2, is a stainless steel needle of 0,8 mm of diameter fixed inside a teflon cylinder. An earthed copper tube of 8 mm of diameter closes the discharge circuit

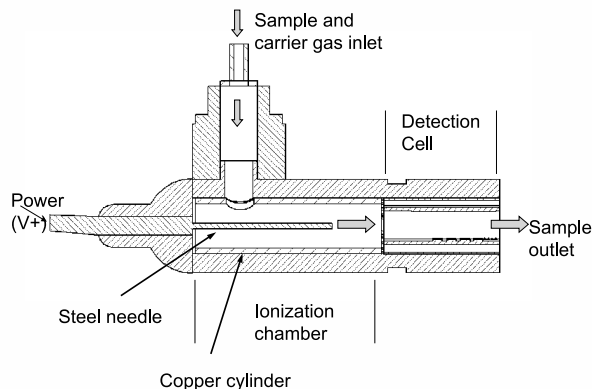


Figure 2: Lateral section of the experimental device. The upper part corresponds to the carrier gas inlet. In the central part ionization is produced, and the detection cell is on the right.

of the pulse. The ionization discharge is recorded with an oscilloscope (Tektronix P6015). The needle is concentric to the copper tube; hence the distance between electrodes is approximately 4 mm. A stainless steel mesh is placed between the ionization chamber and the detection cell in order to screen the high field produced during the ionization discharge within that last zone. The detection arrangement is similar to that proposed by Solis *et al.* [9]; the field  $\vec{E}$  is transversal to the ion flux determined by the carrier gas. Our ion detection device is an assembly of 7 earthed detectors placed in a plane as shown in Fig. 2 and connected to a constant potential which is fixed in the range between 10 and 100V. The dimensions of the detection cell are 17mm  $\times$  11mm  $\times$  2mm. A dry carrier gas of  $N_2$  is used in order to avoid humidity problems in the air (Indura 99,998%,  $H_2O \leq 3\text{mg/ml}$ ). The gas flux is controlled by a flux measuring device: Brooks model 6-658. The testing organic substances are absorbed in a piece of cotton placed in a glass tramp. A flux of  $N_2$  gas passes through the tramp dragging the steam of the sample at room temperature and directed to the ionization zone. The ions generated are dragged by the same flux of  $N_2$  gas towards the detection cell. Each electrode is connected to a resistance of 3.2 M $\Omega$  and the electrical signal generated by the ions is measured in a oscilloscope Instek GDS 810S synchronized with the pulse of the discharge of the ionization needle. All the system is controlled with a PC and due to the high signal/noise relationship, only 8 signals are necessary to average the response of each detector. With this system it is possible to study: Absolute Ethanol (Merck, pro-analysis, 99.8%), Toluene (Mallinckrodt, analytical, 99.8%) and Acetone (Sintorgan, analytical, 99.5%). All of them were used without any previous treatment.

### 3. Numerical simulations

The ion paths in the detection cell were simulated with the SIMION 8.0 code. The SDS module was implemented. This module combines the dynamics of a particle in a viscous medium and its interaction with the carrier gas at room pressure [5]. We give here a brief description of such a simulation. In order to define an ion path, the equation of motion is considered, in which acceleration has a viscosity component due to velocity in Eq.(1), and another Coulombic component due to the electrostatic potential of the cell. Furthermore when the SDS module is implemented, a diffusion model is incorporated. The statistics of the distance covered after  $10^5$  collisions in  $10^5$  ion samples was applied. From the ion-gas mass relationship data of 1, 10, 100, 1000 and 10000, the distance corresponding to intermediate values of mass were calculated by interpolation. Such distance is used to modelling the size of the jump in a step of the path. The direction within the 3D space of the cell should be calculated with a uniform distribution in order to modelling the expected local isotropy. In this sense, an appropriate sample space should be chosen. For instance, if a point within a cube is randomly taken in order to obtain a random direction, the appropriate sample space is defined only by those points that belong to the sphere inscribed in such a cube [14]. Once the path is defined, the algorithm reports the positions of the ion's impact. We have instrumented a couple of codes written in interpretative language (Perl) to process the data accompanying each ion path. With these codes we obtain the charge collected as a function of time. Through a numerical derivation of the collected charge, the current in each detector as a function of the time of flight was obtained.

The SIMION 8.0/SDS algorithm [5] allows us to estimate (from the mass data) or to take as a predetermined information, the mobilities of the ions whose paths will be modeled. Two types of ion path simulations were considered: one without fragmentation and the other with fragmentation. This means that, for each species studied, ions of the whole molecules were considered first, and secondly, the fragments of such molecules according to their relative abundances [15] being the least of them higher than 10%. Fig. 3 shows the surface potential energy view obtained with Simion 8.0 for the simulation of paths considering only primary ions (without fragmentation) of Toluene, Acetone and Ethanol. Results indicate that the ions of Acetone and Ethanol with greater mobility are collected preferentially in the detectors closer to the capture cell inlet (see also Fig. 2).

### 4. Results

In this section, experimental results and numerical simulations of the device proposed here for the detection cell by swept-field scanning are presented. Flight times are analyzed as well as the collected charges in detectors for different combination of carrier gas flux and detector potentials. The analysis of the principal components for one of the selected combinations is also presented.



Figure 3: Surface potential energy view of the ion path simulation of a Toluene (black) - Acetone (light gray) - Ethanol (gray) mixture obtained by Simion 8.0. The ions come from the right top side of figure. The top part of the traces correspond to the potential of needle discharge (5000V). The carrier flux with velocity 30 m/s allows the flow of the ions go into detector zone where potential increments are indicated by the surface potential level. In the left bottom side of figure ions impacts to detector at 0V at the lowest part of the surface potential. The anode is opposite to it in the upper part of the surface potential at 50V.

The experimental results are given in the first subsection, and in the following subsections the results of simulations and numerical calculations are shown.

#### 4.1. Experimental

Under normal conditions of pressure and temperature different tests were performed as described in Section 2 for Acetone, Ethanol and Toluene at saturated steam pressure using the device shown in Fig. 2. The location of the detectors in the detection cell is shown in Fig. 4. Ion gas moves from left to right as

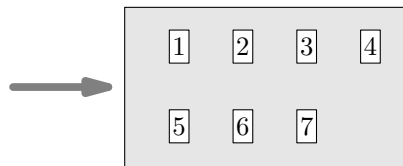


Figure 4: Diagram that shows the numbering for the array of detectors. Ions flux goes into detection cell from the left as indicated by the arrow.

indicated by the arrow. The charge collected during the detection process was obtained for each detector. In Fig. 5 these data for each substance are displayed. According to Eq.(2), the differences in mobility allows to correlate time with position taken by an ion which arrives on a detector. In order to explain experimental results, we need to consider that the mobility of Toluene ( $K_0 = 1,87$ ) is lower than that of Ethanol ( $K_0 = 2,06$ ) and Acetone ( $K_0 = 2,13$ ) [3, 4] and that with the configuration proposed, the electric field is perpendicular to

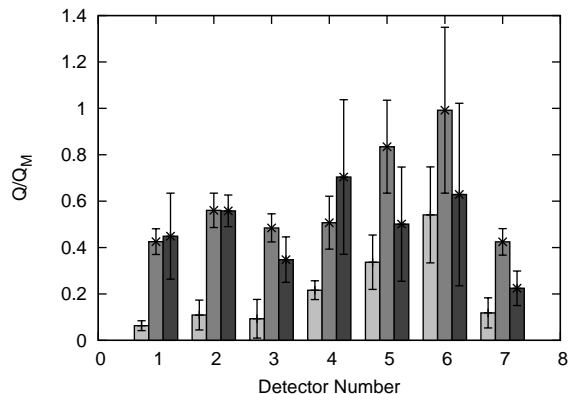


Figure 5: Collected charge measured in each detector when Acetone (light gray), Ethanol (gray) and Toluene (dark gray) samples are tested separately.

the direction of the carrier gas (see Fig. 1). Hence, Toluene ions should travel longer distances without being deviated compared with Ethanol and Acetone ions. For these last ones, the scarce relative difference of 3.5% reported between the Acetone (larger) and Ethanol (smaller) mobilities [3, 4], might yields to similar path deflection and nearly the same distance of impact on detectors produced by the swept-field scanning. In general, it is expected that lighter ions have larger mobilities as they have smaller inertial mass. Although this rule applies for a large number of molecules [3, 4] there are some exceptions where the opposite is true. Such exceptions can be explained in terms of a fragmentation process of the primary ion to lighter secondary ions and, therefore, with greater mobility. Due to the type of ionization proposed in this work, we suppose that the fragmentation of Acetone and Ethanol produce secondary ions with highly relative abundance [16]. Consequently, each species acquire a different mobility compared to that expected in terms of primary ions mass alone.

#### 4.2. Times of Flight

The velocity of the carrier gas and the difference of electric potential within the cell can be conveniently combined in order to modulate the amount of ions that goes to a given place of the experimental device. We shall analyse here the time of flight for each ion and the average rate of the collected charge in each detector as a function of both the velocity of the carrier gas and the difference of electric potential. In Fig. 6 we display the normalized current generated in each detector by the ions of Toluene when the velocity of the carrier gas is 3, 9 and 30 m/s and the differences of electric potential in each detector cell are 15 and 150 V. A pattern that spreads the current over time of flights when both the velocities  $v_g$  and potentials diminishes is observed. This can be explained considering that the contribution to the ion's energy from the interaction between the ions and the carrier gas do compete with the electrical counterpart. Increasing the electric potential differences of the



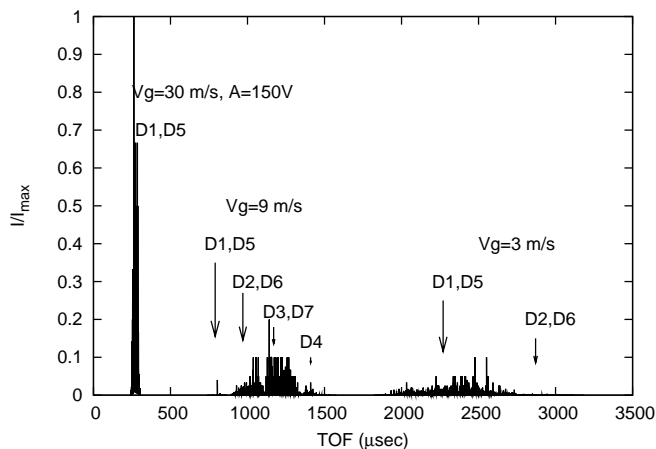


Figure 6: Normalized  $I/I_{max}$  current intensity vs. time of flight (TOF) for each detector  $D_i$  with  $i = 1 \dots 7$  ordered by pairs as shown in the graph labels. For  $v_g = 3$  and  $9$  m/s, the difference of potential is  $A = 15$  V.

cell will give a larger kinetic energy contribution to the ions compared with the contribution from the Brownian motion. Thus, such electric potential increment clearly produce a lesser diffuse and so more defined and stretched ion paths. For that reason, in Fig. 6 it is observed that, as both the velocity of the carrier gas and the potential decrease, the average rate of ions that arrive at the same time also decrease. This means that in such case the ions arrival are expanded over the whole detection zone.

#### 4.3. Collected charges in detectors

Counting the amount of collected charge in each detector offers an alternative way to get the times of flight. Their results are also in agreement with experimental data. We present here the measurement of the collected charge when the velocity of the carrier gas is  $30$  m/s and the difference of potential in the cell is  $50$  V. It is verified that the times of flight are larger for ions that arrive on detectors which are farther to cell inlet. For instance, in Fig. 7 the same graph for detectors  $D_6$  and  $D_7$  is shown for the collected charge  $Q$  divided by total charge  $Q_T$  of ions when Toluene, Acetone and Ethanol are tested separately.

When mobility is estimated from ion mass, as should be if we consider the case of fragmentation process during the ions generation, the charge collected in each detector as a function of time of flight follows the simple rule expected by inertial mass considerations. This can be observed in Fig. 7. The collected charge for Ethanol is greater than that of Acetone for times of flight between  $280$  and  $350 \mu\text{s}$  corresponding to the arrival of ions at the detector  $D_6$ . However, if we consider the mobilities reported in the literature we could expect that this result

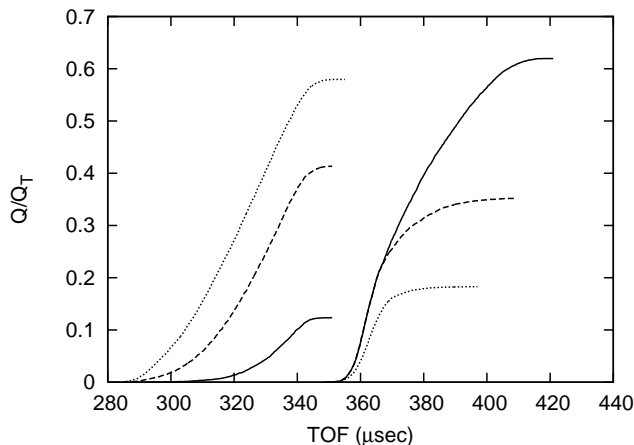


Figure 7: Normalized total charge  $Q/Q_T$  for detectors  $D_6$  (left) and  $D_7$  (right) for each species as a function of time of flight when primary ions were considered for Toluene (full lines), Ethanol (dotted lines) and Acetone (dashed lines).

should be the opposite one. For that reason, we performed our simulation also considering groups of secondary ions. We supposed that when Acetone, Ethanol and Toluene were ionized they would form groups of ions from the fragmentation of the primary ion. We considered the ions with a relative abundance greater than 10%. Furthermore, using secondary ions, we found out a large defocusing and a low temporal definition due to a wide charge distribution on the detectors assembly. Then as an improvement we considered more appropriate to represent the collected charges in each detector taking care also of the secondary ions for each species. In Fig. 8 we display such results. In this case a charge distribution closer to that expected in terms of Acetone ion mobilities is obtained. However, a larger amount of Ethanol ions than that of Acetone ions in detectors ( $D_1, D_5$ ) is still observed. Such detectors are the first pair from the entrance to the cell of the carrier gas. The second pair of detectors is ( $D_2, D_6$ ). For this second pair, the method of secondary ions seems to be more consistent with the expected result in terms of known mobilities. The detector pair that follows is ( $D_3, D_7$ ). In this last case, the result that arise when considering fragmentation is again opposite to that which would be expected from mobilities.

#### 4.4. Principal components analysis

Based on the previous background on simulation and experimental results we are able to do another step forward. Our working assumption is now that once the cell geometry and the operational conditions of our device are given (the carrier gas flux and the cell potential values) the charge collected in each detector has its own statistics for each unknown species. Specifically, the analysis of the principal components applied to our device allows us to determine the

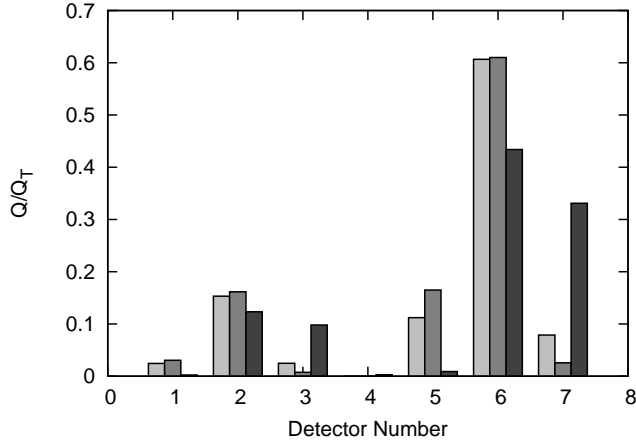


Figure 8: Normalized collected charge  $Q/Q_T$  in each detector obtained from the fragmentation product of the primary ion with relative abundance greater than 10% for Acetone (light gray), Ethanol (gray) and Toluene (dark gray). Over 6000 ion paths are averaged for each species considering carrier gas velocities between 20 and 30 m/s. Numeration and configuration of detectors is the same as that of the experimental device.

fingerprint of each species corresponding to our experimental configuration. We associate a random variable  $X^i$  ( $i = 1 \dots 7$ ) to the collected charge  $Q$  in each detector, normalized with the total charge  $Q_T$  and distributed on all the detectors. Thus,  $X^i$  are real numbers in the interval  $[0, 1]$ . Each measurement of the collected charge in a detector corresponds to an event of the random variable  $X^i$ . Therefore, if we perform  $N$  measurements for each variable, we can construct the vector  $\vec{X}^i = (X_1^i, X_2^i, \dots, X_N^i)^T$  whose coordinates are the result of these measurements. The notation  $(\dots)^T$  means the transpose of  $(\dots)$ . From the definition of the mean value  $\bar{X}^i = 1/N \sum_l X_l^i$  and experimental covariance [17], a real symmetric and covariant matrix  $\mathbf{C}$  is obtained, whose dimension is equal to the number of detectors, *i.e.*  $7 \times 7$ . Their elements are defined by

$$\mathbf{C}_{ij} \equiv Cov(X^i, X^j) = \frac{1}{(N-1)} \sum_m (X_m^i - \bar{X}^i)(X_m^j - \bar{X}^j), \quad (7)$$

where  $m = 1 \dots N$ . We now introduce the similarity transformation

$$\mathbf{D} = \mathbf{P}^T \mathbf{C} \mathbf{P}, \quad (8)$$

where  $\mathbf{D}$  is a diagonal matrix and  $\mathbf{P}$  is an orthogonal matrix containing the eigenvectors of  $\mathbf{C}$  ordered by columns. From the last matrix it is possible to define the transformation

$$\mathbf{Y} = \mathbf{P}^T \mathbf{X}, \quad (9)$$

That enable us to change from random variables of detectors

$$\mathbf{X} = (\vec{X}^1, \vec{X}^2, \dots, \vec{X}^7)^T. \quad (10)$$

to a new set of random variables

$$\mathbf{Y} = (\bar{Y}^1, \bar{Y}^2, \dots, \bar{Y}^7)^T, \quad (11)$$

From this output a principal subgroup can be obtained

$$\mathbf{Z} = \mathbf{Q}^T \mathbf{X}, \quad (12)$$

being  $\mathbf{Q}$  the matrix formed by the first  $n \leq 7$  eigenvectors of  $\mathbf{C}$  ordered in decreasing order of its eigenvalues. The final results

$$\mathbf{Z} = (\bar{Z}^1, \dots, \bar{Z}^n)^T, \quad (13)$$

contain the expected principal components. Different criteria were proposed for getting  $n$  [12], although all of them consider the minor subspace in which the greatest quantity of data is concentrated [13].

The results of Eq.(11) can be understood in terms of a coordinate transformation. Within the new coordinate system, each component is independent. This allows us to define an orthogonal space that represent the data obtained from measurements of collected charges for each species. The principal eigenvectors used show in turn the specific combination of the original detectors that intervene in the output of the measurement.

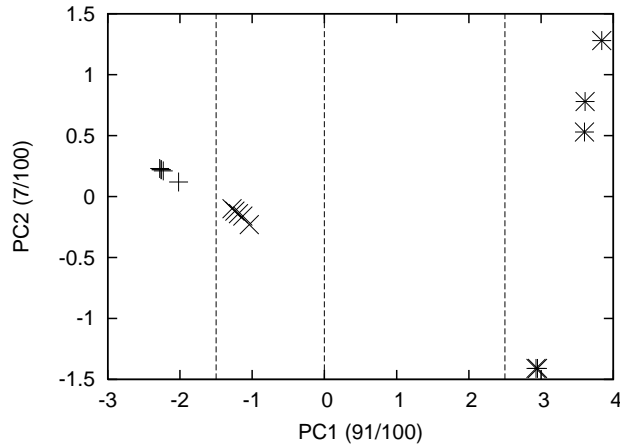


Figure 9: The first two principal components for 5 measurements of the charge collected in each detector when using all of them. Ethanol (plus symbol), Acetone (cross symbol) and Toluene (asterisk symbol) averaged on 6000 runs each species.

Fig. 9 shows the coordinates of the two first principal components for a set of 5 measurements of the collected charge in each detector for Ethanol, Acetone and Toluene ions and fragments of them. Each one of these measurements is similar to that represented in Fig. 8 and corresponds to the average values on a sample of 6000 ion paths, considering the carrier gas velocities between 20 and 30 m/s. Only 2% of data remains outside the analyzed set by the two first

principal components, distributing 91% in the first and 7% in the second of them. Fig. 10 shows the coordinates in the two first principal components of

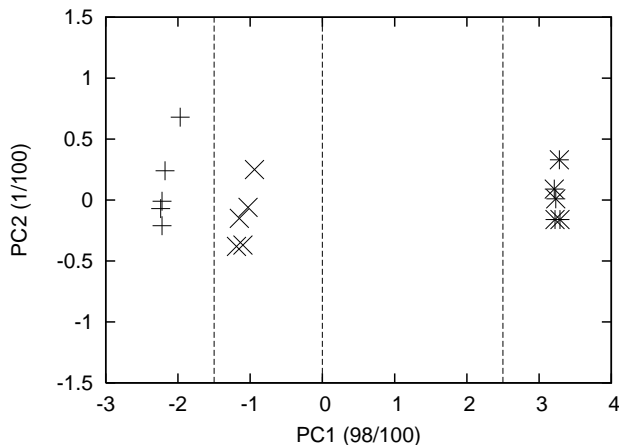


Figure 10: The first 2 principal components for 5 measurements of collected charge in each detector, but without detector number 4. Ethanol (plus symbol), Acetone (cross symbol) and Toluene (asterisk symbol) averaged on 6000 runs each species.

measurements on the same system considered in Fig. 9, but with one variable less due to detector number 4 was not considered. In this case it is observed that 99% of data is represented by the first two components and 98% only by the first one. This is explained by the fact that being very scarce the collected charges on detector 4, as can be seen in Fig. 8, the diminution of the number of variables decreases the dimension of the total space considered with a very little alteration of the sample size. Therefore, the concentration of data in the first two principal components increase. The relevance of the PCA result is considerable regarding the separation of the three set of data for all species we have studied. The identification of an unknown sample is positive if its representation fits within any of the clearly non-overlapping region of our three set of data (see Figs. 9 and 10).

## 5. Conclusions

Our simulation clearly shows that for the trace of ions, the carrier gas velocity and the cell potential are directly correlated. The analysis of fragmented ions partially explain the traces of Acetone and Ethanol when their mobilities are estimated from fragments mass. However, the integrated signals which were obtained experimentally show the same trend that our simulation. As shown in Fig. 5, when comparing the signals of detectors ( $D_1, D_5$ ) with the subsequent pair ( $D_2, D_6$ ), it is observed that they maintain almost the same proportion between all substances for each detector, but the whole amount is increased in the second pair. In the third pair, ( $D_3, D_7$ ), the proportion of the trend

between substances almost remains the same, but decreasing the total amount of the set. Only in the most distant detector the result is different and shows the proportions between species following the expected results in terms of tabulated mobilities [3, 4].

Since the simulations of the times of flight for each substance shows a characteristic distribution for both, charges and currents obtained through the detectors assembly, i.e. a *fingerprint*, the statistical correlation in the distribution of collected charges in the detectors using the Principal Component Analysis can be applied.

For the experimental prototype proposed here a set of specific parameters (velocity of carrier gas and electric potential of the cell) to define Acetone, Ethanol and Toluene traces were optimized by numeric simulation. Afterwards a PCA statistical analysis of the collected ion charges in the set of detectors is used to define a non-overlapping region in a appropriated diagram for each of the above mentioned compounds. Thus, our procedure, which involves a training to develop the proper fingerprint of each compound, can be used in the designing of devices for the identification with certainty of unknown compounds,

## 6. acknowledgment

GPO acknowledge illuminating discussions with W. Luis Mochán and useful comments of Patricio F. Provasi and Rodolfo H. Romero. This work was supported by FONCyT (grant PAE 22592/2004 nodo NEA:23016 and nodo CAC:23831).

## References

- [1] D.S. Moore. Instrumentation for trace detection of high explosives. *Rev. Sci. Instrum.*, 75:2499, 2004.
- [2] H.E. Revercomb and E.A. Mason. Theory of plasma chromatography/gaseous electrophoresis- a review. *Anal. Chem.*, 47:970, 1975.
- [3] M.D. Wessel, J.M. Sutter, and P.C. Jurs. Prediction of reduced ion mobility constants of organic compounds from molecular structure. *Anal. Chem.*, 68:4237, 1996.
- [4] N. Agbonkonkon, H.D. Tolley, M.C. Asplund, E.D. Lee, and M.L. Lee. Prediction of gas-phase reduced ion mobility constants ( $k_0$ ). *Anal. Chem.*, 76:5223, 2004.
- [5] A.D. Appelhans and D.A. Dahl. Simion ion optics simulation at atmospheric pressure. *Int. J. Mass Spectrom.*, 244:1, 2005.
- [6] J.I. Baumbach and G.A. Eiceman. Ion mobility spectrometry: Arriving on site and moving beyond a low profile. *Appl. Spectrosc.*, 53:338A, 1999.

- [7] R.A. Miller, G.A. Eiceman, E.G. Nazarov, and A.T. King. A novel micro-machined high-fiel asymmetric waveform-ion mobility spectrometer. *Sens. Act. B Chem.*, 67:300, 2000.
- [8] K.J. Gillig, B.T. Ruotolo, E.G. Stone, and D.H. Russell. An electrostatic focussing ion guide for ion mobility-mass spectrometry. *Int. J. Mass Spectrom.*, 239:43, 2004.
- [9] A.A. Solis and E. Sacristán. Designing the measurement cell of a swept-field differential aspiration condenser. *Rev. Mex. Fis.*, 52:322, 2006.
- [10] S. Zimmermann, N. Abel, W. Baether, and S. Barth. An ion-focusing aspiration condenser as an ion mobility spectrometer. *Sens. Actuators B*, 125:428, 2007.
- [11] H. Lai, T.R. Mcjunkin, C.J. Miller, J.R. Scott, and J.R. Almirall. The predictive power of simion/sds simulation software for modeling ion mobility spectrometry instruments. *Int. J. Mass Spectrom.*, 2008. to be published.
- [12] K. Pearson. On lines and planes of closest fit to systems of points in space. *Philosophical Magazine*, 2:559, 1901.
- [13] A. Lamagna, S. Reich, D. Rodriguez, and N.N. Scoccola. Performance of an e-nose in hops classification. *Sens. Actuators B*, 102:278, 2004.
- [14] The points of the cube considered by the code SIMION 8.0/SDS in the line 1044 of *collision\_sds.lua* define directions to their corners more likely. Thus, for isotropic case such line code is not correct for local definition of random direction to be model in a step movement on the path of ions.
- [15] P.J. Linstrom and W.G. Mallard, editors. *NIST Chemistry WebBook*. Number 69 in Nist Standard Reference Database. National Institute of Standard and Technology, Gaithersburg MD, 20899, 2005.
- [16] Japan AIST/NIMC Database-Spectrum MS-IW-7880. *Acetone*. NIST Mass Spectrometry Data Center, USA, 2007.
- [17] P.Meyer. *Probabilidad y aplicaciones estadísticas*. Addison-Wesley Iberoamericana, 1986.